American Mineralogist, Volume 59, pages 1299–1318, 1974

Stress and Strain in Cryptoperthite Lamellae and the Coherent Solvus of Alkali Feldspars

PIERRE-YVES F. ROBIN[1]

Department of Earth and Planetary Sciences,
Massachusetts Institute of Technology,
Cambridge, Massachusetts 02139

Abstract

Transmission electron microscope observations of a cryptoperthitic alkali feldspar from Larvik (Norway) show that the exsolution lamellae are fully *coherent,* that is, they maintain full continuity of their lattices across the lamellar interfaces; this confirms X-ray work by previous authors on other crytoperthites.

Coherency imposes elastic strains in individual lamellae, causing the lattice parameters to differ from those of unstrained crystals of the compositions. From known elastic constants and known compositional variation of stress-free lattice parameters, elastic strain and stress components in a lamella are calculated as linear functions of $(X\text{-}X^\circ)$ (where X = mole fraction $KAlSi_3O_8$; X° = average value for bulk crystal). The assumption that elastic strain entails no volume change and the resulting method of determining compositions of individual lamellae (Smith, 1961) can therefore be evaluated; an alternate simple method is proposed, which makes use of the fact that there are linear combinations of two $(h0l)$ spacings which are not affected by the elastic strain.

The elastic strain energy varies as $(X\text{-}X^\circ)^2$. When strain energy is taken into account in the thermodynamic treatment of exsolution, a 'coherent solvus' can be calculated, with a critical temperature 70° to 85°C below the critical temperature of the solvus for unconstrained phases (*e.g.,* Luth and Tuttle, 1966). This agrees well with the hitherto unexplained results of annealing experiments on single crystals by Tuttle and Bowen (1958) and Smith and MacKenzie (1958).

Lamellar exsolution occurs in many other mineral systems. If the lamellae have retained coherency, the relevant phase diagram is the coherent solvus, not the unconstrained one determined in hydrothermal experiments. Other transformations within crystals may also give rise to elastically strained phases coexisting along coherent interfaces. The corresponding strain energy must be taken into account in the thermodynamic analysis and the geologic interpretation of such transformations.

Introduction

Cryptoperthites are lamellar mixtures of exsolved potassium- and sodium-rich alkali feldspars in which individual lamellae are too thin to be resolved optically. Some authors (*e.g.,* Tuttle, 1952) have restricted the use of the name to those mixtures in which lamellae have thicknesses of one μm or more. In accordance with more recent usage, however, the 'cryptoperthites' considered in this paper include Tuttle's cryptoperthites and X-ray perthites.

Lattice parameters of the two feldspars coexisting in a cryptoperthite often do not fit the description of any known homogeneous feldspar. Variations with composition of the lattice parameters of homogeneous crystals in the sanidine-high albite series have been systematically investigated (Donnay and Donnay, 1952; Orville, 1967; Wright and Stewart, 1968) and are therefore quite well known. Typically, however, in the K-rich phase of a cryptoperthite, a "is too long relative to b and c . . ." (Wright and Stewart, 1968). Consequently, compositions of these 'anomalous' phases, as determined by several X-ray methods using different lattice parameters, are contradictory and sometimes physically impossible (Laves, 1952; Coombs, 1954; MacKenzie and Smith, 1956; Smith and MacKenzie, 1958).

[1] Present address: Department of Geology and Erindale College, University of Toronto, Mississauga, Ontario, L5L 1C6 Canada.

Phases coexisting in a cryptoperthite also appear to be anomalous in their exsolution behavior. The existence of a two-phase region in the high-temperature alkali feldspar solid solutions below temperatures of 650°C is well documented (*e.g.,* Bowen and Tuttle, 1950; Orville, 1963; Luth and Tuttle, 1966; Müller, 1971). Thermodynamic equations of state have been derived by several authors (Thompson and Waldbaum, 1968, 1969; Waldbaum and Thompson, 1968, 1969; Luth *et al,* 1970, 1972; Delbove, 1971) and provide a basis for quantitative treatment of exsolution. However, homogenization experiments of sanidine-high albite cryptoperthites (Tuttle and Bowen, 1958; Smith and MacKenzie, 1958) indicate a solvus very significantly lower than the ones determined in hydrothermal experiments. These authors attributed the discrepancy to the fact that they were dealing with natural feldspars, as opposed to the synthetic ones used in hydrothermal work. There has been no further discussion of Tuttle and Bowen's (1958) and Smith and MacKenzie's (1958) results. The experimental work of Müller (1971) shows in fact that for increasing degrees of Al-Si order, as expected in natural feldspars, the critical temperature becomes higher, not lower, than for the disordered high-temperature solution series synthesized in the laboratory.

Many, perhaps most, optically homogeneous high-temperature alkali feldspars of intermediate compositions occurring in nature are cryptoperthites. The present author also believes that most perthites are derived from an earlier cryptoperthitic state. The questions raised by cryptoperthites are therefore important for alkali feldspars in general. The purpose of this paper is to show that cryptoperthite lamellae are, in many cases, *coherent lamellae,* and that *coherent lamellar exsolution* quantitatively explains the lower solvus discussed above.

The anomalous cell parameters of cryptoperthite phases were qualitatively explained by Laves (1952) and Smith (1961). These authors observe that the repeat distances are equal in both phases along [010] and along an irrational direction between [106] and [108]. The plane which [010] and this irrational direction define corresponds to the orientation determined for the *Schiller* plane exhibited by many moonstones, and to the direction of microperthite lamellae observed optically. Both Laves and Smith concluded that the two phases of a cryptoperthite exsolve as lamellae approximately oriented between $(\bar{6}01)$ and $(\bar{8}01)$ but *maintain continuity of their lattices along their interfaces.* The anomalous parameters result from the elastic strain necessary to satisfy this constraint. Smith (1961) further notes that, in homogeneous crystals, [106] is the direction in the *ac* plane along which the repeat distance is affected least by changes in composition. Smith therefore suggests that the lamellae are oriented as observed in order to minimize the required elastic strain.

Cryptoperthite lamellae have been observed in transmission electron microscopy (TEM) (Fleet and Ribbe, 1963; Bollmann and Nissen, 1968; Brown, Willaime, and Guillemin, 1972; Willaime and Gandais, 1972; Willaime, Brown and Gandais, 1973). TEM observations essentially confirm the lamellar structure postulated by Laves and by Smith, with, however, some complexities when the K-rich phase has partially or totally inverted to triclinic symmetry (Brown *et al,* 1972). Further explanations of the orientation of the lamellae are given by Bollmann and Nissen (1968), using the *O-lattice theory,* and by Willaime and Brown (1972) and Willaime (1973) using computer calculations of strain energy in bi-crystals made of equal amounts of both phases. Orientations predicted do not differ significantly from the one given by Smith (1961).

Coherency

A boundary between two phases across which the two lattices are in continuity is often referred to as a *coherent boundary* or *coherent interface,* and an exsolving phase which maintains coherent interfaces with its matrix is accordingly called a *coherent precipitate* (*e.g.,* Kelly and Nicholson, 1963). Coherent exsolution lamellae may be considered simply as coherent precipitates with a much larger extent in two dimensions than in the third.

The requirement that two phases meet along coherent interfaces generally sets up nonhydrostatic stresses in each phase. At a given temperature the Helmholtz energy of a chosen mass of the stressed phase differs from its value under a hydrostatic pressure P by an amount called the *strain energy.* The strain energy is the mechanical work performed by stresses on the mass of the phase to bring it, at constant temperature, from P to its nonhydrostatically stressed state. During coherent exsolution strain energy results in a 'penalty' against exsolution into two phases; the extent of the two-phase field is there-

fore reduced compared to the *hydrostatic solvus.*[2] Cahn (1962) first noted this fact and developed the theory of coherent phase diagrams for exsolution (coherent solvus) for the case of elastically isotropic precipitate and matrix, and isotropic stress-free transformation strain. Christie (1968), Yund and McCallister (1970) and Willaime (1973) mention the possible existence of a coherent solvus in alkali feldspars.

The derivation of the coherent solvus presented in this paper is exact under the following assumptions:

(i) All phases have the same degree of Al-Si order as sanidine.

(ii) All phases have monoclinic symmetry. For the part of the calculation which applies to room-temperature conditions, this assumption can only be justified by the fact that the Na-rich phase is regularly twinned in such a way as to simulate monoclinic symmetry. For the calculation of the coherent solvus the analysis can be taken to apply exactly only to that part of the solvus at temperatures above the monoclinic-triclinic transition of the Na-rich phase (a restriction similar to that of Thompson and Waldbaum, 1969). A consequence of monoclinic symmetry is that the stress and strain tensors considered have one principal axis along the *b* axis (diad axis), the two other principal axes being in the *ac* plane.

(iii) All relative changes of lattice parameters, whether due to changes in composition or to elastic deformation, are small enough to be considered infinitesimal. The assumptions of infinitesimal strain and of linear elasticity greatly simplify the calculations and the representation of strain.

(iv) Each lamella, characterized by a definite set of stress-free lattice parameters, is bounded by two infinite parallel coherent boundaries. The thickness of the composite 'book' of lamellae is much larger than the thickness of an individual lamella, and there is no systematic variation in the bulk composition of the crystal (as averaged over many lamellae) when moving along a direction perpendicular to the lamellae. A very important property of such lamellae can be stated as follows:

> If no average stress other than hydrostatic is applied on the boundaries of the composite, stresses and strains are uniform within each lamella. There are no shear stresses on the lamellae boundaries. The stress normal to the boundaries is equal to the hydrostatic stress applied onto the composite. The other two principal components of stress are parallel to the boundaries and vary with the composition of the lamella.

This result is demonstrated in Appendix A.

In reality lamellae are not infinite in their own plane, and stresses and strains are not uniform in regions near the edges of a lamella or near the external boundaries of the crystal. Calculations of stress, elastic strain, and strain energy based on the assumption of infinite parallel lamellae are nevertheless probably applicable if thicknesses of individual lamellae are less than, say, one tenth of their planar extent.

(v) Surface energy is neglected. Coherent interfacial energy (which will be a further penalty against exsolution) is generally considered low. Ardell (1968, 1970) calculated specific interfacial energies of 14 and 21 erg cm^{-2} for coherent γ' particles in Ni-Al and Ni-Ti alloys, respectively. In feldspars the distance between two adjacent alkali-ion sites, the only sites whose population changes across an interface, is large ($\simeq$5 Å) compared to equivalent distances in the alloys studied by Ardell. Thus the interfacial energy in feldspars could be even lower than in alloys (Ardell and Nicholson, 1966). For an average lamellar thickness of 0.2 μm, a specific interfacial energy of 20 erg cm^{-2} amounts to 2 cal mol^{-1} and can reasonably be neglected. For higher values of interfacial energy and/or smaller lamellar thicknesses the total surface energy may become important.

Transmission Electron Microscopy (TEM)

TEM samples were prepared from petrographic thin sections by ion bombardment thinning (Heuer *et al,* 1971) and examined with a 100 kV JEM (Japan Electron Microscope) and a Siemens 101 with tilting stages. The crystals studied are from a gray-blue larvikite of the M.I.T. collection, merely identified as being from Larvik, Norway. Feldspars from this general area have been studied in detail, particularly by Oftedahl (1948), Muir and Smith (1956), and Smith and Muir (1958). Some specimens have been examined in TEM by Bollmann and

[2] The term hydrostatic is often used in this paper to contrast with coherent. Thus the *hydrostatic solvus* is the equilibrium exsolution curve for unconstrained phases, which are therefore under hydrostatic pressure. The *hydrostatic equation of state* is the equation of state of uniform homogeneous unconstrained phases.

Nissen (1968), Willaime and Gandais (1972) and Willaime *et al* (1973).

The feldspar studied here exhibits a light blue 'schiller'; its composition [mole fraction X = Or/(Ab + Or)] varies from $X = 0.09$ to $X = 0.74$ within a single polished thin section, and averages $X = 0.34$. This lack of homogeneity is confirmed by TEM observations. 'Large' regions (several tens of square microns) consist entirely of albite which is twinned according to the pericline law (Fig. 1). Other regions, although still mostly albite, contain irregular lamellae of K-feldspar (Fig. 2). We note (Fig. 2) that the periodicity of pericline twinning in albite is variable. Willaime and Gandais (1972) report a relationship between periodicity of albite twinning and thickness of albite lamellae in cryptoperthites; a similar relationship appears to be true here for pericline twinning.

Most of the crystal, however, is characterized by a dense alternation of K- and Na-rich lamellae. Figure 3 is a good example of the lamellar structure to which the elastic analysis of the following section can be applied. As in Figures 1 and 2, the view is along the *b* axis, and the plane of the micrograph is the *ac* plane. Because pericline twinning corresponds to a 180° rotation of the albite lattice about the *b* axis, the two twin orientations give rise to only one set of diffraction spots; the other set of spots (Fig. 3b) belongs to the K-feldspar. Most individual lamellae

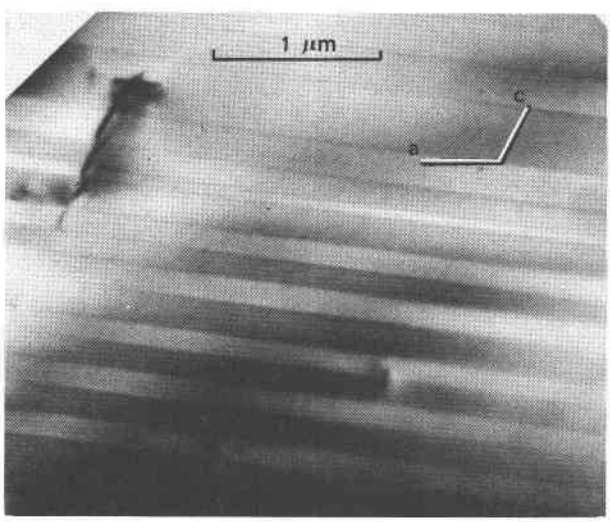

FIG. 1. 'Large' region of larvikite alkali feldspar consiting solely of albite, regularly twinned according to the pericline law. Three isolated lattice dislocations are visible. The view is along the *b* axis. 100 kV, Japan Electron Microscope.

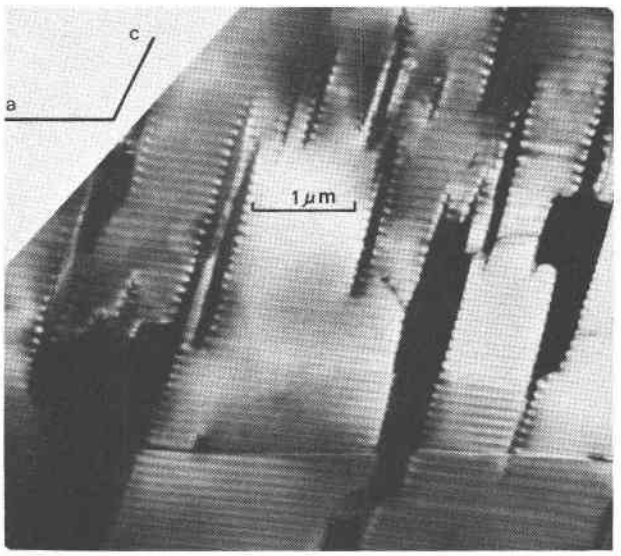

FIG. 2. Irregular exsolution lamellae of K-feldspar, showing as dark areas. The periodicity of pericline twinning (alternating shades of gray) is variable. The view is along the *b* axis. 100 kV, JEM.

are more than ten times as long as they are thick, their longest direction (**IP**, Fig. 3) making a 107° angle with the basal cleavage.

The noticeable variation in intensity within a lamella is a result of *strain contrast*: inhomogeneous strain causes variations in deviation from the Bragg condition for the electron beam, and hence variations in intensity of the transmitted beam. This inhomogeneous strain may seem incompatible with the property of uniformity demonstrated in Appendix A; however, it is in fact chiefly due to the thin slicing necessary for TEM observations. Indeed, consider a slice of crystal approximately perpendicular to the plane of the lamellae and whose thickness is comparable to or smaller than the thickness of individual lamellae. The assumption of infinite extent, acceptable for the original crystal, is no longer valid; slicing allows a non-uniform relaxation of the original stresses and gives rise to the inhomogeneous strain observed.

Stresses along some directions cannot be relaxed, however; if boundaries between lamellae are co-

We note (Fig. 3b) that the line segments between two points of same index, corresponding to the K- and Na-feldspars, are all parallel to each other and perpendicular to the lamellae boundaries in real space. It is shown in Appendix B that such a relationship, exemplified in Figure B1, is a general property of the reciprocal lattices of coherent lamellae.

Therefore, although the strain contrast of Figure 3a does not permit detection of possible mismatch dislocations along the boundaries, the diffraction pattern can be taken as sufficient evidence that the lamellae are coherent.[3]

The absence of mismatch dislocations is confirmed by an oblique view of lamellae boundaries under high magnification (Fig. 4); Moiré fringes herent, repeat distances along the lattice direction **IP** are still maintained equal in the two types of lamellae. In other words, the constraint of coherency is not relaxed for these lattice planes which are parallel to the axis of the microscope and give rise to the diffraction pattern of Figure 3b.
(*e.g.,* Hirsch et al, 1965) are visible, but no dislocations can be imaged.

TEM thus demonstrates that the crytoperthite lamellae studied here are coherent, as were those examined by Laves and by Smith. Not all cryptoperthites are necessarily coherent however; Aberdam and Kern (1962) and Aberdam *et al* (1964) observed 0.1 to 1.1 μm thick lamellae whose boundaries were semi-coherent, that is, they exhibited regularly spaced *mismatch dislocations*. The analysis of elastic stresses and strains which follows only applies to those cryptoperthites which have preserved full coherency.

Elastic Analysis

Although actual calculations are lengthy, the method of obtaining elastic stresses and strains in individual lamellae is straightforward. Known changes of the stress-free lattice parameters of high-temperature alkali feldspars are used to calculate the strain components imposed on a lamella of composition X (mole fraction $KAlSi_3O_8$) which exsolves from a crystal of average bulk composition X° but retains coherency with it. From Hooke's law the stress and the remaining strain components can then be calculated as a function of $(X - X^\circ)$.

Stress-Free Compositional Strain

Although lattice parameters do not vary exactly linearly with X, a linear approximation is sufficient here; because the data will be applied to exsolution, tangential values at the anticipated critical composition are preferable. Slopes of tangents at $X = 0.33$ can be measured directly from Orville's (1967) curves[4]:

$$\frac{1}{b}\frac{\partial b}{\partial X} = 0.0162, \qquad (1)$$

$$\frac{1}{a}\frac{\partial a}{\partial X} = 0.0567, \quad \frac{1}{c}\frac{\partial c}{\partial X} = 0.0112, \quad \frac{\partial \beta}{\partial X} = 0.0116.$$

A change in lattice parameters is a strain. Within the

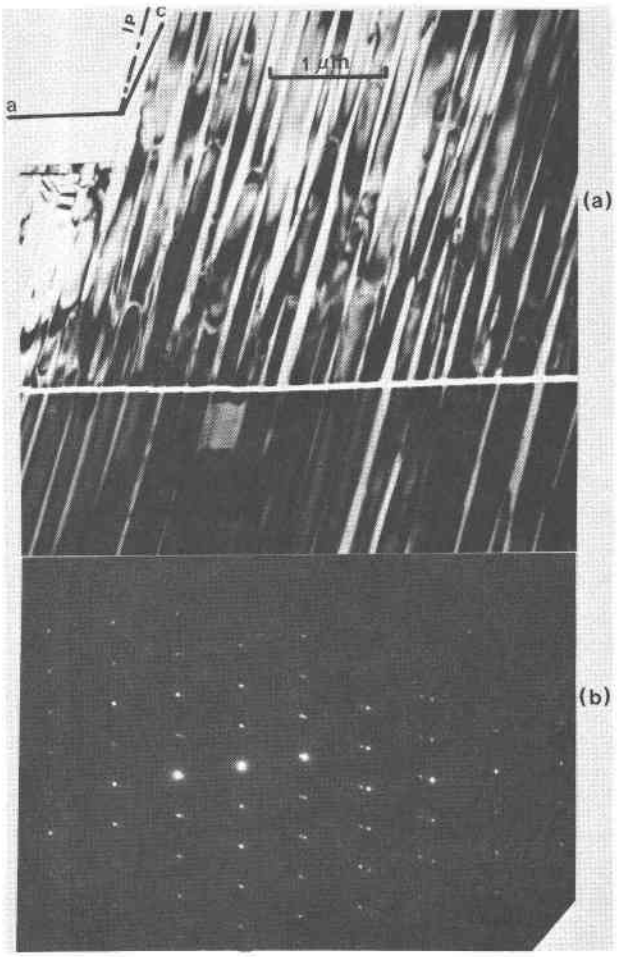

FIG. 3. **(a)** Direct image of lamellar structure. Lamellae make an angle of 107° with the basal cleavage. **(b)** Electron diffraction pattern. 100 kV, JEM.

[3] The diffraction pattern of Figure 3b satisfies the relationship of Figure B1 because the two pericline twins give rise to only one set of diffraction spots. For other orientations, or other twin laws, the situation is more complicated; in case of coherency, only mid-points between two twin spots bear the relationship to the K-feldspar spots which is shown in Figure B1. The two twin spots themselves lie on a line perpendicular to the twin boundaries in real space.

[4] The triclinicity of the albite phase is ignored; in all rigor, when that phase is twinned according to the pericline law, a and c should be replaced by $1/a^*$ and $1/c^*$. Similarly, had the albite been twinned according to the albite law, b should be replaced by $1/b^*$. The difference is insignificant here.

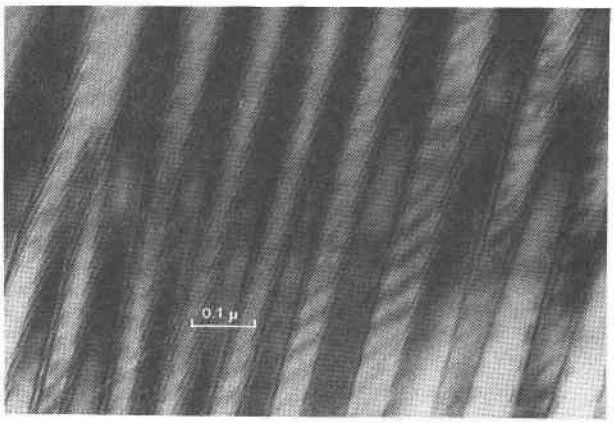

FIG. 4. Thin exsolution lamellae viewed under high magnification. Moiré fringes mark the lamellae boundaries, which are here viewed at an angle. The undulations visible in every other lamella are probably due to twinning of the sodium-rich phase. Siemens 101 Electron Microscope.

approximation of monoclinic symmetry, the stress-free compositional strain coefficients in Eq. 1 are sufficient to determine the *stress-free compositional strain* (or, for short, *compositional strain*) completely. The intermediate principal axis of strain is along the *b* axis. Compositional strain in the *ac* plane is conveniently represented (Fig. 5) by its *Mohr circle* (see Nye, 1957). The minimum principal axis of strain (point **m**) makes an angle of approximately 110° with the *a* axis, and the corresponding minimum longitudinal strain coefficient is equal to 0.0105. The maximum longitudinal strain coefficient is 0.0630 (point **M**). The Mohr circle construction thus verifies Smith's (1961) observation that the direction of the contact plane of cryptoperthites corresponds closely to a minimum in compositional expansion. Computations of strain energy by Willaime and Brown (1972) should in principle give a more exact prediction of the orientation of the lamellae. In practice, however, longitudinal strain components enter as squared quantities in the expression of strain energy, while elastic coefficients can be verified numerically not to be very sensitive to small rotations of axes; the orientation minimizing the strain energy should therefore be close to the one containing the minimum and intermediate principal axes of compositional strain.

Choice of Coordinates

Cartesian coordinate axes are chosen with the 1-axis normal to the lamellae boundaries, the 2-axis along the crystallographic *b* axis, and the 3-axis normal to 1 and 2 (Fig. 6). Rather than take 110°, predicted by Figure 5, as the angle between the contact plane and the *a*-axis, 107° is chosen, more in

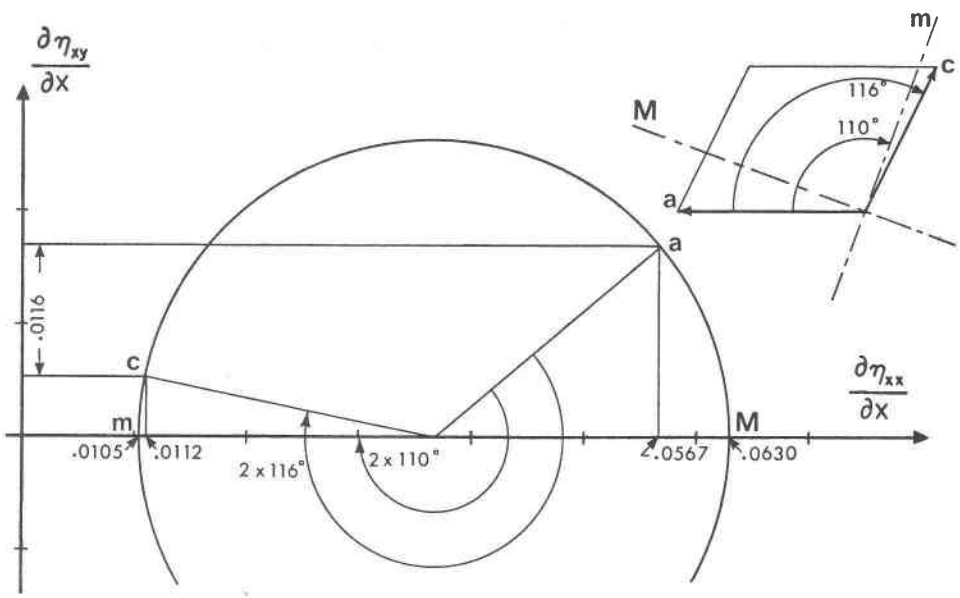

FIG. 5. Mohr circle for the stress-free compositional strain in the *ac* plane. Abscissas of *a* and *c* and the difference between their ordinates are given by Eq. 1. The angle between the *a* and *c* axes is then sufficient to construct the Mohr circle. **m**: direction of the minimum principal axis of compositional strain; **M**: maximum principal axis.

line with observed values. The new coordinate axes are approximately the principal axes of compositional strain and are related to the conventional coordinate system for monoclinic crystals by a rotation of 17° about the b-axis. Let us call η_{ij} the stress-free compositional strain. In our system of coordinates the compositional strain coefficients are therefore

$$\frac{\partial \eta_{22}}{\partial X} = 0.0162,$$

$$\frac{\partial \eta_{11}}{\partial X} = 0.0630, \frac{\partial \eta_{33}}{\partial X} = 0.0105, \frac{\partial \eta_{13}}{\partial X} \simeq 0.$$

Now, if we take the unstressed lattice of a homogeneous crystal with an arbitrary composition $X°$ as reference state, the compositional strain of a crystal of composition X, with respect to that reference state, is,

$$\eta_{22} = 0.0162(X - X^0), \tag{2a}$$

$$\eta_{11} = 0.0630(X - X^0),$$

$$\eta_{33} = 0.0105(X - X^0), \eta_{13} \simeq 0, \tag{2b}$$

$$\eta_{11} + \eta_{22} + \eta_{33} = 0.0897(X - X^0). \tag{2c}$$

Elastic Constants

The only published values of elastic constants for alkali feldspars are by Ryzhova and Aleksandrov (1965), henceforth called R&A, who measured acoustic velocities in crystals of various compositions. The reported constants show no systematic variation with composition and are therefore taken to be independent of the latter. The non-systematic variations of the constants are large, however, and are probably due, as Simmons (1964), R&A, and Christensen (1966) point out, to cleavages and other flaws in the crystals. Two approaches are taken to correct for these imperfections: (1) Feldspar No. 61 of R&A exhibits a relatively high absolute value of all its stiffness constants; thus estimated to be a relatively flawless crystal, its elastic constants are taken as a first set. (2) A second set, C, is generated by choosing for the c_{ij} the highest value calculated by R&A for all the alkali feldspars they studied (including an albite reported by Ryzhova, 1964).

The two sets, reported for the conventional coordinate system, are given in Table 1. Their values, recalculated for the new coordinate system (Voigt, 1928, p. 593), are also given in Table 1. As a way to estimate the uncertainty of the results due to the uncertainty of our knowledge of the elastic constants, all calculations are carried out with the two sets of constants. Numerical results are given for each set, the ones corresponding to set C being given in parentheses.

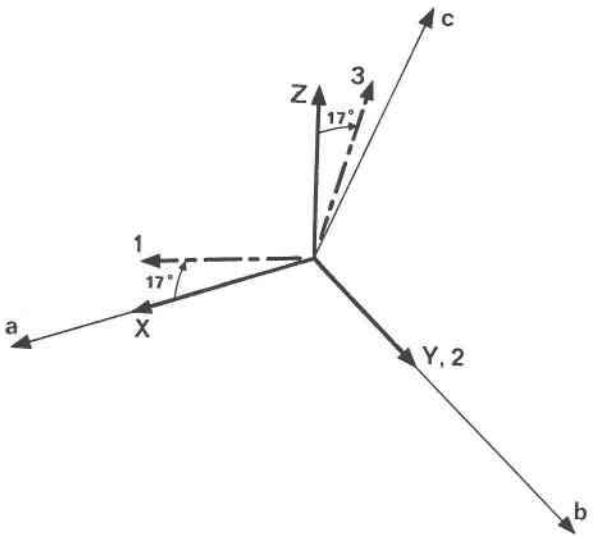

FIG. 6. Coordinate systems. a, b, c: conventional crystallographic axes for a monoclinic feldspar (b = diad axis). X, Y, Z: conventional cartesian coordinate axes. 1, 2, 3: present choice of cartesian coordinate axes.

Stresses and Strains

Let us now consider a cryptoperthite, of average composition $X°$, made up of many coherent exsolution lamellae. The elastic strain components imposed on a lamella of composition X are

TABLE 1. Selected Stiffness Constants of Alkali Feldspars[1]

c_{ij}	11	22	33	44	55	66
	12	13	23	15	25	35	46
No. 61[2]	0.596	1.581	1.049	0.139	0.203	0.370
	0.362	0.360	0.285	-0.118	-0.057	-0.129	-0.026
C[3]	0.750	1.720	1.280	0.170	0.300	0.370
	0.430	0.490	0.360	-0.170	-0.140	-0.190	-0.030
No. 61[4]	0.493	1.581	1.145	0.173	0.207	0.336
	0.324	0.364	0.326	-0.050	-0.069	-0.028	-0.086
C[4]	0.615	1.720	1.457	0.204	0.279	0.336
	0.346	0.469	0.444	-0.054	-0.136	-0.096	-0.081

[1] *Elastic constants measured by acoustic methods are adiabatic constants; the correction from adiabatic to isothermal is not large enough to be significant. Units are Mbar.*

[2] *Ryzhova and Aleksandrov (1965), Table 3. Conventional coordinates.*

[3] *Composite set of elastic constants from Ryzhova and Aleksandrov (1965), Table 3, and from Ryzhova (1964). Conventional coordinates.*

[4] *Elastic constants recalculated in new coordinate system, illustrated in Figure 6.*

$$\left.\begin{aligned}\epsilon_2 &= \epsilon_{22} = -\eta_{22} = -0.0162(X - X^0),\\ \epsilon_3 &= \epsilon_{33} = -\eta_{33} = -0.0105(X - X^0),\\ \epsilon_4 &= 2\epsilon_{23} \simeq 0.\end{aligned}\right\} \quad (3)$$

That is, the lamella is elastically constrained to match the lattice of the 'average crystal' across the coherent boundary plane. Equations 3 are rigorously exact only to the extent that compositional strain coefficients and elastic constants are independent of composition.

Elastic strain and stress components are related by Hooke's law, which, for our purpose, can be written (matrix notation; see Nye, 1957):

$$\sigma_1 = \sigma_4 = \sigma_5 = \sigma_6 = \epsilon_4 = \epsilon_6 = 0, \quad (4a)$$

$$\left.\begin{aligned}\sigma_2 - c_{12}\epsilon_1 - c_{25}\epsilon_5 &= c_{22}\epsilon_2 + c_{23}\epsilon_3,\\ \sigma_3 - c_{13}\epsilon_1 - c_{35}\epsilon_5 &= c_{23}\epsilon_2 + c_{33}\epsilon_3,\\ - c_{15}\epsilon_1 - c_{55}\epsilon_5 &= c_{25}\epsilon_2 + c_{35}\epsilon_3,\\ - c_{11}\epsilon_1 - c_{15}\epsilon_5 &= c_{12}\epsilon_2 + c_{13}\epsilon_3.\end{aligned}\right\} \quad (4b)$$

The solution of Eq. 4b, using numerical values from Eq. 3 and from Table 1, is

$$\sigma_{22} = \sigma_2 = -0.0230(X - X^0) \text{ Mbar}, \quad (5a)$$
$$(-0.0257)$$

$$\sigma_{33} = \sigma_3 = -0.0106(X - X^0) \text{ Mbar}, \quad (5b)$$
$$(-0.0140)$$

$$\epsilon_{11} = \epsilon_1 = +0.0182(X - X^0), \quad (5c)$$
$$(+0.0164)$$

$$2\epsilon_{13} = \epsilon_5 = -0.0024(X - X^0), \quad (5d)$$
$$(-0.0083)$$

where the parentheses denote values calculated for the elastic constants of set C (see Table 1).

The volumetric strain is

$$\epsilon_1 + \epsilon_2 + \epsilon_3 = -0.0085(X - X^0). \quad (5e)$$
$$(-0.0103)$$

If a hydrostatic pressure P is acting on the crystal, the lattice of the homogeneous crystal X° under the pressure P may be taken as a new reference state. In that case, Eqs. 3, 5c, and 5d still give the elastic strain components provided the effect of pressure on compositional strain coefficients and elastic constants can be neglected (an assumption to be justified later). The principal stress components σ_1, σ_2, and σ_3 are increased by $-P$ over their values in Eqs. 4b and 5a, b.

Composition Determinations From Lattice Parameters

Equations 3 and 5 determine all the components of elastic strain in a lamella of composition X coherent within a crystal of average composition X°. The various methods of determining compositions from X-ray lattice parameters can therefore be evaluated.

Figure 7 is the Mohr circle for the elastic strain in (010). It shows that the $(\bar{2}01)$ spacing, $d_{(\bar{2}01)}$, is *elastically increased in the K-rich lamellae* $[(X - X^\circ) > 0]$ and *elastically decreased in the Na-rich lamellae* $[(X - X^\circ) < 0]$. Consequently, if $d_{(\bar{2}01)}$ is used without precautions to determine compositions, the K-rich lamellae will be found richer in potassium and the Na-rich lamellae poorer than either really are. If their real compositions are already close to

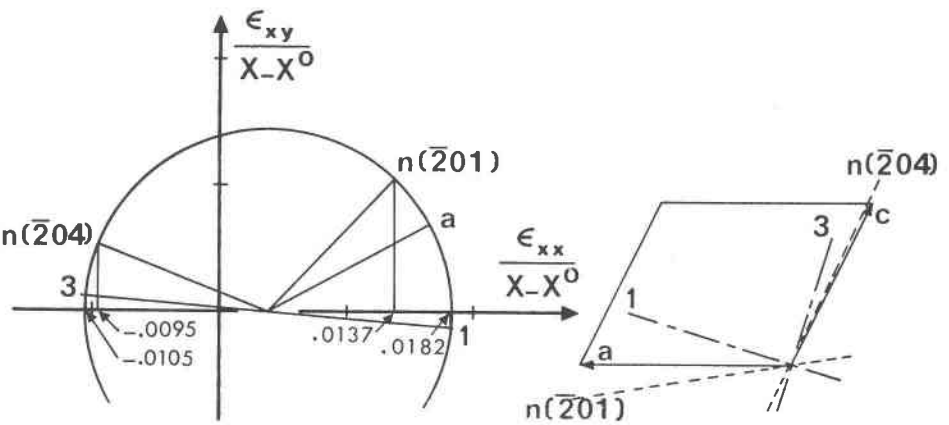

FIG. 7. Mohr circle for elastic strain in the *ac* plane. The relative change of $d_{(h0l)}$ spacing is equal to the longitudinal strain ϵ_{xx} in a direction normal to $(h0l)$, noted here $n_{(h0l)}$. (Elastic constants of R&A's crystal No. 61).

end members, the $d_{(\bar{2}01)}$ method may thus yield physically impossible results such as $X > 1$ or $X < 0$ as reported by Coombs (1954).

Figure 7 shows that, contrary to $d_{(\bar{2}01)}$, $d_{(\bar{2}04)}$ is elastically *decreased* in the K-rich lamellae and *increased* in the Na-rich ones. There is a linear combination of $d_{(\bar{2}01)}$ and $d_{(\bar{2}04)}$ which is neither increased nor decreased by the elastic strain (Appendix C); such linear combination is therefore a *function of composition alone* and can be used to determine the composition of the lamellae.

Smith (1961) suggested the use of the volume of the lattice cell to determine compositions of cryptoperthite lamellae, under the assumption that this volume is unaffected by elastic strain, *i.e.*, that $\epsilon_1 + \epsilon_2 + \epsilon_3 = 0$. In fact, when the lamellae are coherently maintained within a large crystal, the variation of the cell volume with composition is no longer given by Eq. 2c as implied by Smith; this variation must be corrected by the elastic volume change given by Eq. 5e. Comparison of Eqs. 2c and 5e shows that Smith's assumption leads to an underestimate of X for the K-rich phase and to an overestimate for the Na-rich phase, by approximately $0.1(X\text{-}X^\circ)$. If X° is known, the appropriate correction can thus be made. However, such method of determining compositions is unnecessarily complicated.[5]

Wright and Stewart (1968, p. 71) state that, whenever they observe anomalous cell parameters, "*b*, *c*, or both are *too low* relative to *a* to define a consistent structural state." Considerations presented here indicate in fact that if both phases have the Al-Si order of sanidine, Wright and Stewart's statement is true only for the K-rich phase; the Na-rich phase on the contrary has its *b* and *c* cell dimensions 'stretched', and therefore *too large* relative to *a*. Wright and Stewart's statement may stem from the fact that "the character of the sodium phase is usually much more poorly known" (Wright and Stewart, 1968, p. 72). Also, the average composition X° of a cryptoperthitic feldspar is usually closer to that of the albite phase than to that of the K-feldspar; the elastic distortion of the albite should thus be less important and more likely to escape attention.

Because cryptoperthite lamellae are too thin to be resolved by standard microprobe techniques, direct chemical analysis will require a combination of micro-analysis and electron microscopy (*e.g.*, Lorimer and Champness, 1973). In the meantime, methods which use lattice parameters and which take elastic strain into account are probably sufficient. In powders, however, the smallest grain size (say 10 μm) may not always sufficiently exceed the thickness of the largest lamellae (up to 1 μm or more) to prevent some non-uniform stress-relaxation. One would thus expect a broadening of the diffraction peaks and a corresponding loss of accuracy. This danger is probably small for lamellar thicknesses of 0.2 μm or less.

Total Strain

Equations 2 give the stress-free compositional strain η_{ij}. Equations 3, 4b, and 5c,d give the elastic strain ϵ_{ij}. The two strains can be added to give the total strain e_{ij} of a lamella X with respect to an unstrained crystal of composition X°. It is an *invariant plane strain* (see Appendix B). The *total strain between coherent lamellae* X^a and X^b is therefore given by

$$\left.\begin{aligned} e_{22} &= e_{33} = 0, \\ e_{11} &= \underset{(0.0794)}{0.0812}(X^a - X^b), \\ e_{13} &= \underset{(-0.0042)}{-0.0012}(X^a - X^b). \end{aligned}\right\} \qquad (6)$$

Figure 8 is the Mohr circle (in the *ac* plane) for the total strain between the lamellae as constructed from Eq. 6. Point **3** corresponds to the direction of the 3-axis, that is the direction of the contact planes. In general, other lattice directions do not have the same orientation in the two kinds of lamellae; the angular deviation of a direction [*p*0*r*] between the two lattices is given by the difference between its ordinate and the ordinate of point **3** in Figure 8. If this angular deviation is plotted *vs* the angle which [*p*0*r*] makes with the *a* axis, a sine curve is obtained, similar to the curve measured experimentally by Laves (1952). The amplitude of the sine curve is equal to the diameter of the Mohr circle of Figure 8

[5] Jan Tullis (1973, personal communication) has developed another method of obtaining compositions of coherent cryptoperthite lamellae by correcting X-ray lattice parameters for the elastic strain. Her elastic analysis is more exact than the one given here as it does not assume that elastic moduli and compositional strain coefficients are independent of composition. The method J. Tullis suggests is therefore, in principle, more accurate than the one presented in Appendix C; although more complicated, it should become valuable when our knowledge of the elastic constants of alkali feldspars improves sufficiently to warrant the added accuracy.

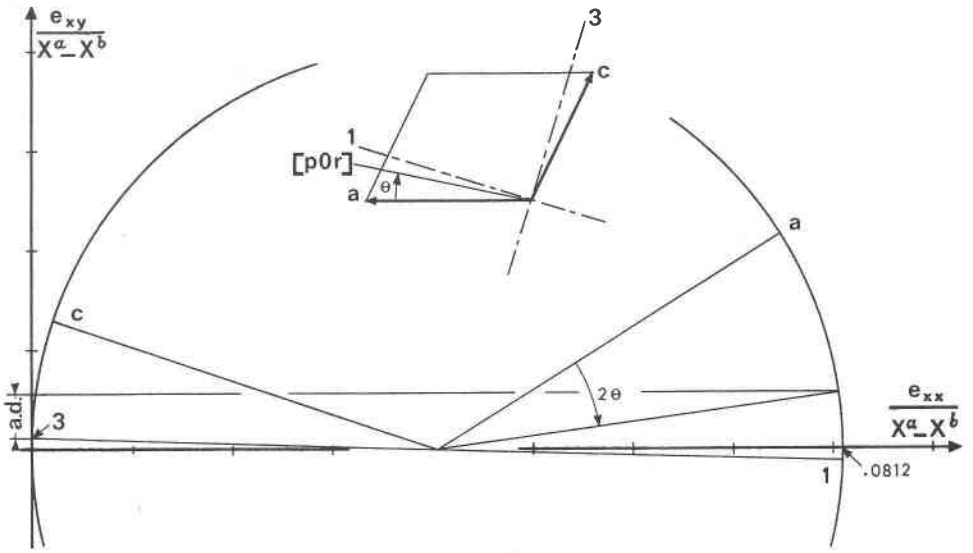

FIG. 8. Mohr circle for total strain between lamellae in the *ac* plane. The segment **a.d.** is equal to the angular deviation of a lattice direction [*p*0*r*] between the two lattices in cryptoperthites. (Elastic constants of R&A's crystal No. 61).

multiplied by $(X^a - X^b)$. In Laves' (1952) Figure 16, the amplitude is 0.068; we conclude that the composition difference in the crystal he studied was

$$X^a - X^b = 0.838(0.857).$$

Elastic Strain Energy

The Helmholtz elastic strain energy in a lamella X is the mechanical work necessary to bring the lamella from a state of hydrostatic pressure P to its nonhydrostatically stressed state at constant temperature. This elastic strain energy is given by

$$\Delta \check{F} = -P(\epsilon_1 + \epsilon_2 + \epsilon_3) + \tfrac{1}{2}(\sigma_2\epsilon_2 + \sigma_3\epsilon_3), \qquad (7)$$

where $\check{F}$ is the Helmholtz energy per unit volume, ϵ_i are the elastic strains, and σ_2, σ_3 are the nonhydrostatic stress components which are added to the pressure P and are given by Eqs. 5a, b. If we take $\bar{V} = 2.5$ cal bar^{-1} mol^{-1} for the molar volume of alkali feldspars, and use Eqs. 3 and 5a, b, c, the molar strain energy can be calculated:

$$\Delta \bar{F} = -P\,\Delta \bar{V}^{el} + k(X - X^0)^2, \qquad (8)$$

where $k = 603.6$ (704.6) cal mol^{-1} and $\Delta \bar{V}^{el}$ is the molar colume change due to elastic strain.

Effects of Pressure and Temperature

Pressure and temperature can affect our results by changing the compositional strain coefficients and by changing the elastic constants.

Strains brought about by a hydrostatic pressure of 5 kbar (for R&A's No. 61), are, in our coordinates

$$\epsilon_2 = -0.00125 \quad \text{and} \quad \epsilon_3 = -0.00137. \qquad (9)$$

Similarly, thermal expansions expected from a rise in temperature to 605°C (analbite, Stewart and von Limbach, 1967) are

$$\epsilon_2 = +0.0033 \quad \text{and} \quad \epsilon_3 = +0.0034. \qquad (10)$$

Only the variations of these quantities with composition contribute to hydrostatic compositional strain. We have already noted that elastic constants do not depend greatly on compositions; variations in the numerical values in Eq. 9 with composition will therefore be negligible compared to the corresponding compositional strain coefficients. There are no complete thermal expansion data for alkali feldspars other than pure albite. However, values of thermal expansion of a sanidine to 605°C are not likely to differ from the ones in Eq. 10 by more than 0.001 (corresponding to a 30 percent difference in thermal expansion coefficients); even then, corrections on $\partial\eta_{22}/\partial\mu$ and $\partial\eta_{33}/\partial\mu$ would only amount to 6 and 10 percent respectively.

The only complete study of the effect of both pressure and temperature on the elastic constants of a silicate is the one of Frisillo and Barsch (1972) on various crystals of bronzite. For a 5 kbar pressure increase, their data indicate a relative *increase* in

value of the C_{ij} between 2.5 and 4 percent for $i = j \leq 3$, between 1.5 and 2 percent of $i = j \geq 4$, and 5 to 10 percent for $i \neq j$. For $i = j$ the stiffness coefficients *decrease* by 9 to 15 percent when temperature is increased to 600°C.

Simmons (1964) measured compressional wave velocities under confining pressure in various minerals, among them a microcline, and noted a rapid increase in these velocities as confining pressure was raised from 0 to 2 kbar. Simmons attributed this increase to crack closure resulting from the pressure increase. Christensen's (1966) observation that this effect was much more pronounced for propagation directions normal to the major cleavages of a perthite and an albite reinforced Simmons' conclusion. Thus, stiffness constants measured at room pressure may be significantly lower than the intrinsic values for flawless crystals; however, the room pressure velocities measured by R&A generally equal or exceed the 2 kbar values obtained by Christensen. The crystals used by R&A must therefore have been of higher quality than Christensen's, and the correction for cracks may accordingly be much smaller.

For other minerals, only equivalent isotropic elastic properties are usually studied as a function of pressure and temperature. Temperature has the most pronounced effects and may decrease the bulk modulus (stiffness) by as much as 15 percent between room temperature and 600°C.

In conclusion, temperature will only affect compositional strain coefficients by 10 percent at most in an unknown sense. Temperature may decrease the stiffnesses by as much as 15 percent. On the other hand, intrinsic values of these stiffnesses may be higher than the ones used here (Table 1) by an unknown amount and are increased further by pressure. Altogether, the net effect of pressure and temperature on our numerical results should not exceed 20 percent; this is less than the present uncertainty in the values of elastic constants of alkali feldspars.

Coherent Solvus

Possible Mechanisms during Coherent Exsolution

Diffusion of alkali ions through the framework structure and coherent boundary migration are mechanisms which are necessary for the development of a crytoperthite. These mechanisms may not occur at significant rates at room temperature. When studying the coherent solvus, however, we are concerned with the equilibrium reached when the above mechanisms are possible.

It is essential to note that, of the mechanisms which are usually assumed possible in heterogeneous equilibrium studies, not all are possible during cryptoperthite formation. Anomalous parameters can only be maintained by nonhydrostatic stresses. It is clear that if all species could diffuse without constraints, the structure would behave like a fluid rather than like a solid and could support no stresses at equilibrium. In fact the thermodynamic description of a stressed solid requires making a distinction between *solid components,* unable to diffuse through the solid, and *fluid components* which describe the possible changes in composition (Gibbs, 1906, p. 215–218; see also Robin, 1974a, for a more extensive discussion).

During cryptoperthite exsolution, Na and K cations are able to diffuse through the feldspar framework. On the other hand, constraints on the other constituents of the silicate framework are such that no independent long-range diffusion of the corresponding chemical species permits the destruction of the framework itself; in fact, site constraints are such that even Na and K do not migrate independently. Therefore, if no Ca is present, there is only one independent fluid component.

The alkali feldspar formula can be chosen as solid component; that is, the number of moles of the solid component in any given volume of crystal is equal to the *sum* of the number of moles (gram formula weight) of $KAlSi_3O_8$ and that of $NaAlSi_3O_8$. (That this component is solid is better understood with the remark that N lattice cells of the crystal contain $4N$ moles of that component, independently of any possible strain of the lattice or of any variation in composition.) The variable composition can be described by the mole fraction X of $KAlSi_3O_8$.[6]

The fundamental equation of state of the solid is then of the form (Gibbs, 1906, Eq. 468)

$$\mathrm{d}\bar{E} = T\,\mathrm{d}\bar{S} + \bar{V}\sigma_{ij}\,\mathrm{d}e_{ij} + \mu\,\mathrm{d}X, \qquad (11a)$$

whereby

[6] In all rigor the fluid component implied by the choice of X as descriptive variable is KNa_{-1}, while the corresponding solid component is $NaAlSi_3O_8$. Indeed, when expressed in terms of these two components the $NaAlSi_3O_8$ content of an alkali feldspar is, paradoxically, constant and independent of the 'actual' composition of the feldspar:

$$K_xNa_{1-x}AlSi_3O_8 = (KNa_{-1})_x(NaAlSi_3O_8)_1.$$

$$\mu = \left(\frac{\partial \bar{E}}{\partial X}\right)_{\bar{S}, e_{ij}}. \tag{11b}$$

$\bar{E}$, $\bar{S}$, and $\bar{V}$ are respectively molar energy, entropy, and volume (the mole being of the solid component); e_{ij} is the total strain (which can be defined only because of the maintenance of the unbroken framework).

The constraint of coherency of the interfaces amounts to the further requirement that the framework be maintained even when a phase boundary migrates through it; the equilibrium condition of coherent interfaces is given by Robin (1974a).

In this section, the strain energy (Eq. 8) and Thompson and Waldbaum's (1969) 'hydrostatic' equation of state are combined into the equation of thermodynamic equilibrium of coherent interfaces. The coherent solvus can then be determined exactly.

Equilibrium Conditions

At equilibrium we must have (Gibbs, 1906, p. 215)

$$\mu^a = \mu^b = \text{constant throughout the system.} \tag{12}$$

The condition of equilibrium of the interfaces (Robin, 1974a, Eq. 18) reduces to

$$(\bar{F}^a + P\bar{V}^a) - (\bar{F}^b + P\bar{V}^b) = \mu(X^a - X^b). \tag{13}$$

Although Eq. 13 may look familiar, it should be pointed out that $-P$ is only one component of the stress tensor, the one acting normal to the boundaries, and that there is only one chemical potential. If $\bar{G}$ is the molar Gibbs energy of the feldspar of same composition X, at the same temperature, and under the hydrostatic pressure P alone, we have

$$\bar{F} + P\bar{V} = \bar{G} + \Delta\bar{F} + P\,\Delta\bar{V}^{el}. \tag{14}$$

We may define the function $\bar{\phi} = \bar{F} + P\bar{V}$. From Eqs. 8 and 14,

$$\bar{\phi} = \bar{G} + k(X - X^0)^2. \tag{15}$$

The energy function $\bar{\phi}$ can be represented on an energy-composition diagram (Fig. 9). Although the applicability of $\bar{\phi}$ to coherent equilibrium had to be established quite differently, $\bar{\phi}$ is quite similar to the function defined by Cahn (1962). In fact the expression of $\bar{\phi}$ reduces to that given by Cahn when the same assumptions of isotropic elasticity and isotropic compositional strain are made; only then, however, does the strain energy become independent of the shape of the precipitate (Crum, cited by Nabarro, 1940). The function $\bar{\phi}$ will therefore be designated here as the *Cahn energy*.

It is shown in Appendix D that under the present constraint of coherency

$$\left(\frac{\partial \bar{\phi}}{\partial X}\right)_{T,P} = \left(\frac{\partial \bar{E}}{\partial X}\right)_{\bar{S}, e_{ij}} = \mu \tag{16}$$

Conditions of equilibrium 12 and 13 are therefore equivalent to a *rule of common tangent* (Fig. 9). Figure 9 provides, in fact, an intuitive explanation of the phenomenon of coherent exsolution; the strain energy term, $k(X - X^0)^2$, can be regarded as the thermodynamic "cost" of coherency when a lamella exsolves within a crystal of average composition X^0. The Cahn energy $\bar{\phi}$ is specific to one bulk composition X^0. As Cahn (1962) pointed out, however, the coexisting compositions are independent of X^0, because, in

$$\bar{\phi} = \bar{G} + kX^2 - 2kX^0X + kX^{0^2},$$

the last two terms do not affect the abscissae of the points of tangency. We also see that because the parabola $k(X - X^0)^2$ is concave upward, compositions of coexisting coherent lamellae always lie in the range between the compositions of coexisting feldspars in hydrostatic equilibrium under the pressure P and at the same temperature. In other words, the coherent solvus is always inside the hydrostatic solvus.

Determination of the Coherent Solvus

Thompson and Waldbaum (1969) and Luth, Martin, and Fenn (1972) find that alkali feldspar solid solutions are adequately described by a Margules expansion of $\bar{G}$ of the form

$$\bar{G} = X_1\mu_1{}^0 + X_2\mu_2{}^0 + RT(X_1 \ln X_1 + X_2 \ln X_2) + (W_1X_2 + W_2X_1)X_1X_2 \tag{17}$$

where $X_2 = X$, $X_1 = 1 - X$, and W_1 and W_2 are linear functions of P and T. Thompson (1967) expresses analytically the rule of common tangent for such an equation of state. When the same algebraic treatment is performed on $\bar{\phi}$ (Appendix E), we find that the system of two equations yielding the coexisting compositions at a given P and T is formally identical to Thompson's (1967) Equations 81, with the difference that W_1 and W_2 must be replaced by $(W_1 - k)$ and $W_2 - k)$.

Thompson and Waldbaum's (1969) expressions of W_1 and W_2 (in cal mol^{-1}) become, for an arbitrarily chosen pressure of 1 kbar,

$$W_1 = 6420 - 4.632\ T,$$

$$W_2 = 7784 - 3.857\ T.$$

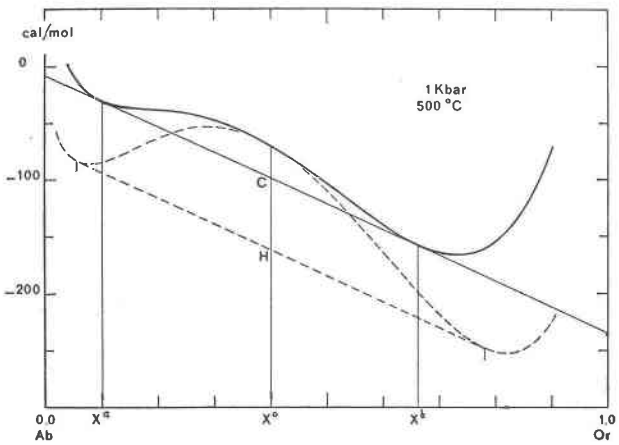

FIG. 9. Energy-composition curves. The dashed curve is a plot of $\bar{G} - X_1\mu_1^0 - X_2\mu_2^0$ using the equation of state of Thompson and Waldbaum (1969). The solid curve is a plot of $\bar{\phi} - X_1\mu_1^0 - X_2\mu_2^0$, for $k = 603.6$ cal mol^{-1} (No. 61). Note that the slope of the common tangent to the $\bar{\phi}$ curve is a function of X^0.

To obtain the coherent solvus at 1 kbar we must use

$$W_1 - k = 5816 - 4.632\ T, \quad (5715)$$

$$W_2 - k = 7180 - 3.857\ T. \quad (7079)$$

The corresponding binodal curves are shown in Figure 10. For the hydrostatic solvus, at a pressure of 1 kbar, the critical conditions are

$$X_c = 0.3334,$$

$$T_c = 934.64\ \text{K} = 661.5°\text{C}.$$

For the coherent solvus under the same P, on the other hand,

$$X_c = 0.3274 \quad (0.3264),$$

$$T_c = 862.23\ \text{K} = 589.1°\text{C}. \quad (850.14\ \text{K} = 577.0°\text{C})$$

Depending on the choice of elastic constants for alkali feldspars we therefore predict a critical temperature for the coherent solvus which is 72°C to 85°C below the critical temperature for the hydrostatic solvus.

Comparison with Experimental Observations

Tuttle and Bowen (1958, Table 2 and Figs. 7 and 9), henceforth called T&B, report a series of experiments in which they maintained several sanidine-high albite cryptoperthites ($0.42 < X^\circ < 0.55$) at successively higher temperatures for long periods of time, and determined the compositions of the coexisting lamellae from their ($\bar{2}01$) spacings. In all cases the crystals had become homogeneous at 610°C. Although T&B had no runs between 550°C and 610°C, they estimated a critical temperature of 570°C. T&B's cryptoperthite solvus broadens very rapidly with lowering temperature and is therefore not entirely contained within the hydrostatic solvus, whereas a coherent solvus should be. However, Smith and MacKenzie (1958)—S&M—questioned T&B's use of the ($\bar{2}01$) method for composition determinations of cryptoperthites. S&M carried out similar experiments and used α^* and γ^* to determine the composition of the sodium-rich phase in their

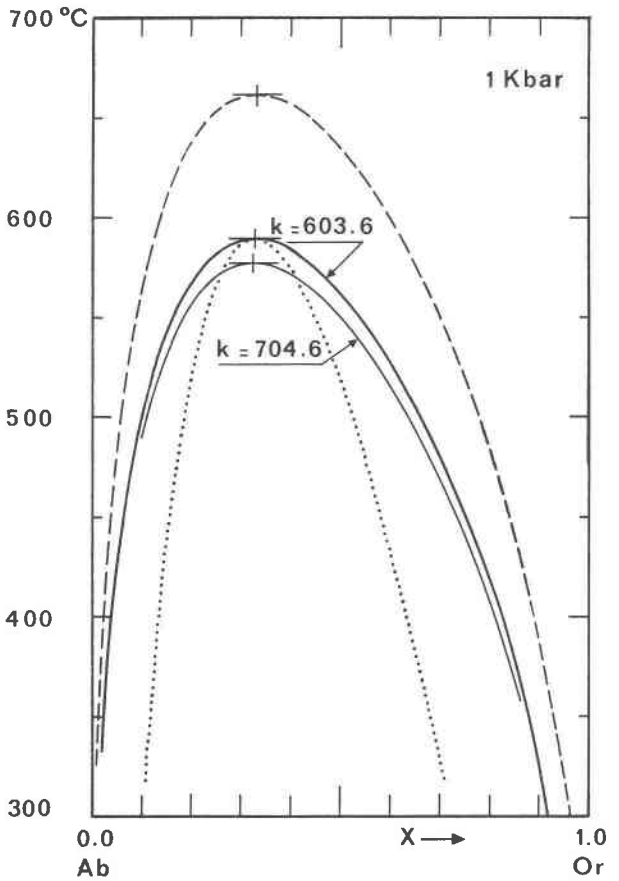

FIG. 10. Temperature-composition diagram. The dashed curve is the hydrostatic solvus at 1 kbar. The solid curves are the coherent solvi corresponding to the elastic constants of R&A's crystal No. 61 ($k = 603.6$ cal mol^{-1}) and of C ($k = 704.6$ cal mol^{-1}). The dotted curve is the spinodal for $k = 603.6$ cal mol^{-1}.

samples and in those of T&B. The solvus they consequently drew (S&M, Figs. 3 and 4) has the same critical temperature, $T_c = 570°C$, but is much narrower than that of T&B; it is entirely contained within any of the various room pressure hydrostatic solvi given by Bowen and Tuttle (1950), Orville (1963), Luth and Tuttle (1966) and Müller (1971).

As shown earlier (Fig. 7 and related discussion), composition determination by the $(\bar{2}01)$ method exaggerates the potassium-content of the K-rich phase and underrates that of the Na-rich phase in cryptoperthites. It therefore leads to too broad a solvus. S&M's curve should therefore be preferred, although coherency stresses may also affect the parameters α^* and γ^* of the twinned albite.

The agreement between the critical temperature inferred from experimental data and the theoretical result presented above is surprisingly good. This agreement strongly suggests that the observed coherency of cryptoperthite lamellae is indeed a sufficient cause for their abnormal exsolution behavior.

Discussion

Uniqueness of Coherent Solvus

Elastic constants and compositional strain coefficients have been assumed to be independent of compositions, thus leading to a constant value of the coefficient k in Eq. 8. Because the compositional strain coefficients in particular are not quite constant, a more refined analysis would result in k being replaced by some linear function of X and X^0. By performing the calculations of Appendix E on the function $\bar{\phi}$ so obtained, it is easy to see that the coherent solvus would no longer be independent of the average composition X^0. The importance of this effect has not been explored.

Coherent Spinodal

The coherent solvus gives the compositions of coexisting lamellae X^a and X^b *in equilibrium* within the constraint of coherency; the two types of lamellae are in particular fully equilibrated with respect to alkali-ion exchange. Let us now consider a homogeneous crystal of composition X^0 whose temperature has been lowered so as to bring it within the coherent solvus. If, furthermore, X^0 is within the coherent spinodal at that temperature, any arbitrarily small fluctuations in composition within the crystal are energetically profitable and thus occur spontaneously. The coherent spinodal, therefore, refers to the *bounds to the average composition* X^0 of an unstable phase *within which the mechanism of coherent spinodal decomposition is possible*; it should not be confused with the coherent solvus.

Because the lattice framework remains unbroken, the energy associated with a coherent composition fluctuation also includes a strain-energy term. To the extent that fluctuations can be considered to be along the 1-direction alone (that is, they preserve the symmetry of Appendix A), the relevant energy function is still the Cahn energy $\bar{\phi}$ given by Eq. 15. The coherent spinodal can thus be calculated from the condition $(\partial^2\bar{\phi}/\partial X^2)_{P,T} = 0$, or $(\partial^2\bar{G}/\partial X^2)_{P,T} = -2k$, and is shown in Figure 10.

'End Regions'

The coherent two-phase equilibrium, like the stress analysis on which it is based, assumes infinite parallel lamellae. Figures 3 and 4, however, show that the lamellae thin out and end, or, conversely, fork. In the 'end-regions,' the stress and strain components and the strain energy are not uniform. The strain energy in particular is higher than in the idealized lamellar structure. Boundary migration and diffusion will thus continue in such regions and lead to a closer and closer approximation of that idealized structure. This expansion or regression of lamellae along their edges must be an important mechanism leading to their overall thickening.

Loss of Coherency

Although the coherent solvus is a stable solvus within the constraint of coherency, the loss of coherency (when possible) leads to a lowering of the total free energy. For example, at 500°C, 1 kbar, and $X^\circ = 0.40$ (Fig. 9), loss of coherency lowers the average free energy by 63 cal mol^{-1} (segment CH, Fig. 9). To the extent that loss of coherency is considered possible, our coherent equilibrium is therefore only a metastable equilibrium. It may happen on the other hand that unconstrained feldspars do not nucleate; in such case the strained cryptoperthite would set higher activities for the feldspar components and could thus cause metastable growth of other phases. We note that the activities of Or and Ab at a given temperature depend on the average composition X° of the cryptoperthite (Fig. 9).

Evolution of Cryptoperthites

We can now sketch the cooling history of a high-temperature alkali feldspar as follows:

(i) composition fluctuations and spinodal decomposition;
(ii) formation of discrete lamellae having sharp boundaries;
(iii) thickening of these lamellae, together with gradual readjustment of their compositions as temperature drops;
(iv) monoclinic-triclinic transition of the albite phase and consequent twinning;
(v) monoclinic-triclinic transition of the potassium feldspar and consequent twinning.

Except for the displacive transition in Na-rich phases, the monoclinic transition in alkali feldspars is accompanied by Al-Si ordering and by large changes in dimensions of the lattice cell. The temperatures of these transitions are therefore likely to be strongly affected by the constraint of coherency and may be quite different from corresponding temperatures in single phase crystals.

The above sequence of events can be quenched at any stage by rapid cooling (except again for the displacive transition in Na-rich phases). On the contrary, long term annealing at a sufficiently high temperature will allow a loss of coherency. Cryptoperthites are thus not found in large batholiths but are instead restricted to extrusive rocks or small intrusive bodies in which cooling must have been slow enough to permit alkali-ion diffusion, but fast enough to prevent nucleation and growth of unstrained phases. There are intermediate situations where a cryptoperthitic feldspar coexists with unstrained phases, the latter growing at the expense of the former. Several examples of coexisting macroperthites and cryptoperthites described in the literature—*e.g.* Moorhouse (1959): Plate 3-D and Fig. 159-B; Tschermak (1864), Brogger (1890), both reproduced by Barth (1969, Figs. 1–15 and 1–16)—can be interpreted in this manner.

Other Minerals

The analysis presented here can be extended to other mineral systems in which coherent exsolution may occur.

Plagioclase Feldspars

The peristerite solvus of sodium-rich plagioclases is a likely candidate. Indeed peristerites have many features in common with cryptoperthites. The Schiller effect which they exhibit was first interpreted by Laves (1951) as due to the coexistence of two plagioclase phases. Typical end-member compositions are An_2 and An_{22} (wt percent of the $CaAl_2Si_2O_8$ component) with rather large variations (*e.g.,* Ribbe, 1960). Fleet and Ribbe (1965) observed almost perfect peristerite lamellae in TEM. Although Fleet and Ribbe interpreted the electron diffraction patterns as the superposition of normal reciprocal lattices for the two end-member compositions (their Fig. 4), the actual patterns (their Fig. 2) are better interpreted as two anomalous reciprocal lattices which satisfy the relationship of Figure B1. Indeed anomalous lattice parameters have been recorded in peristerites, and Viswanathan and Eberhard (1968) assigned the anomalies to 'distortion'. Korekawa, Nissen, and Phillip (1970) studied an oligoclase ($An_{16.5}$) by X-ray and TEM, and interpreted the lattice-parameter fluctuations observed as composition fluctuations; in the present terminology the latter would be called coherent (compare in particular their Figure 5 with the present Figure B1). Korekawa *et al* may thus have observed an early coherent spinodal decomposition stage of peristerite formation. Coexisting single-phase crystals of albite and oligoclase have been observed by Evans (1964) and Crawford (1966) and thus evidence the existence of a hydrostatic peristerite solvus. Iiyama (1966) observed the three-phase field sanidine-albite-oligoclase experimentally and determined that the crest of the peristerite solvus was between 700° and 800°C. The three distinct phases observed by X-rays in some single crystals (Viswanathan and Eberhard, 1968) may in fact be the coherent counterpart of the hydrostatic three-phase field.

Schiller effect and lamellar structures are also observed for more Ca-rich plagioclases and have been interpreted as exsolution lamellae; X-ray and TEM results are difficult to interpret, however.

Clinopyroxenes

Robinson *et al* (1971) noted that the assumption of continuity of lattices between host and lamellae in clinopyroxenes readily explained observed orientations of the lamellae in natural pyroxenes. TEM observations of lunar pyroxenes (Christie *et al,* 1971) are also fully compatible with coherency of the lamellae. Clinopyroxene exsolution may thus well be a coherent process in many cases, as suggested by Champness and Lorimer (1971). A more extensive discussion of the coherency of clinopyroxene exsolution lamellae is given by Robin (1974b).

Exsolution lamellae are observed in many other

mineral systems; however, only a detailed study can determine in each case whether these lamellae are coherent or not.

Coherency, strain energy, and their thermodynamic implications have wider applications than to coherent exsolution. If two or more phases coexist within an unbroken lattice framework and are thus compelled to match along coherent interfaces, they in general acquire a strain energy which they would not have if coherency were not maintained. If, as in this paper, the phases can be considered to be in equilibrium with respect to well-defined mechanisms (migration of fluid components, cation ordering, displacive strain), the inclusion of strain energy in the thermodynamic analysis of such transformations is in principle straightforward. Such analysis is clearly required if these phase equilibria are to be used as reliable geothermometers or geobarometers.

Appendix A: Uniformity of Stresses and Strains within Lamellae

Consider a set of lamellae which satisfy the following conditions:

1. The lattice framework behaves elastically; that is, it is not broken or disrupted by the stresses.
2. Boundaries between lamellae are coherent.
3. The boundaries are infinite, parallel planes.
4. Each lamella is characterized by a definite set of stress-free lattice parameters which is a function of its composition.
5. The thickness of the 'book' of lamellae is much larger than the thickness of an individual lamella, and there is no systematic variation in the composition of the crystal (as averaged over many lamellae) when moving along a direction perpendicular to the lamellae.

We choose a cartesian coordinate system such that the 1-axis is perpendicular to the plane of the lamellae, the 2- and 3-axes being therefore parallel to the lamellae boundaries.

Because of Condition 3, the origin in the 2,3 plane is arbitrary, and thus

$$\sigma_{ij,2} = 0, \quad \sigma_{ij,3} = 0, \quad \text{for } i, j = 1, 2, 3,$$

where

$$\sigma_{ij,k} = \partial\sigma_{ij}/\partial x_k.$$

The three equations of equilibrium reduce to

$$\sigma_{1i,1} = 0, \qquad \text{for } i = 1, 2, 3.$$

Hence, σ_{11}, σ_{12} and σ_{13} are constant throughout the composite. If only a hydrostatic pressure P is applied to the external boundaries, $\sigma_{11} = -P$ and $\sigma_{12} = \sigma_{13} = 0$.

Similarly, because of Conditions 1, 2 and 3, compatibility equations (*e.g.*, Sokolnikoff, 1956, p. 28) reduce to

$$e_{22,11} = 0, \qquad e_{33,11} = 0, \qquad e_{23,11} = 0, \qquad \text{(A1)}$$

where the strain, e_{ij}, can be of compositional as well as elastic origin and $e_{ij,kl}$ denotes $\partial^2 e_{ij}/\partial x_k\,\partial x_l$.

Within a lamella of constant composition (Condition 4) any strain variation must be of elastic origin. Eqs. A1 then become (in matrix notation)

$$\begin{bmatrix} S_{22} & S_{23} & S_{24} \\ S_{23} & S_{33} & S_{34} \\ S_{24} & S_{34} & S_{44} \end{bmatrix} \times \begin{bmatrix} \sigma_{2,11} \\ \sigma_{3,11} \\ \sigma_{4,11} \end{bmatrix} = \begin{bmatrix} 0 \\ 0 \\ 0 \end{bmatrix}. \qquad \text{(A2)}$$

The assumption of linear infinitesimal elasticity is made in Eq. A2; the result demonstrated here is more general however. A demonstration for finite strain and nonlinear elasticity would require care in defining instantaneous stress, strain and elastic constants.

All eigenvalues of a symmetric matrix of elastic coefficients, such as in Eq. A2, are positive; otherwise there would be combinations of non-zero stresses for which the strain energy would be zero or negative, which is impossible. The determinant of Eq. A2 is therefore non-zero, and the only solution to Eq. A2 is the trivial one:

$$\sigma_{2,11} = \sigma_{3,11} = \sigma_{4,11} = 0. \qquad \text{(A3)}$$

Stress components σ_{22}, σ_{33} and σ_{23} can therefore only vary linearly with x_1 within a lamella. The sense along the 1-axis is arbitrary (Condition 5), and, therefore, by reason of symmetry, σ_{22}, σ_{33} and σ_{23} are constant within lamellae. They do not have the same value in lamellae of different compositions, however.

Part of the theorem demonstrated here is a special case of a more general theorem given by Eshelby (1957). Eshelby shows that if no stresses are applied at infinity, stresses and strains are uniform within coherent ellipsoidal inclusions. (Eshelby does not use the term coherent; in the present terminology, however, the problem he treats is the one of coherent inclusions.) In the general case, only one phase, the inclusion, can be surrounded by an ellipsoid. Under the conditions of this appendix, where ellipsoids are reduced to the two parallel planes bounding a lamella, the distinction between host and inclusion disappears: Eshelby's result consequently applies to all lamellae.

Appendix B: Reciprocal Lattices of Coherent Lamellae

Consider a crystal made of lamellae of only two distinct compositions and satisfying conditions 1 to 5 of Appendix A. (In Appendix A the number of possible lamella compositions is not restricted to two). Each lamella is in a homogeneous state of strain and lattices in all lamellae of one kind are superposable by a parallel translation. The two lattices, corresponding to the two kinds of lamellae, are related to each other by a unique linear transformation which must leave the plane of the boundaries invariant, a direct consequence of the constraint of coherency. The linear transformation is thus an *invariant plane strain* (IPS) —See Wayman (1964). A classic result of linear transformation theory is that linear transformations can be

characterized in general by three distinct *eigenvectors* and associated *eigenvalues*. An eigenvector is a vector whose direction is unchanged in the transformation; its eigenvalue is the ratio of the length of the transformed vector to the original. In an IPS, any two non-collinear vectors in the invariant plane (IP) can be arbitrarily chosen as eigenvectors, and their corresponding eigenvalues are 1. Unless the transformation is an identity, the third eigenvector of an IPS is not arbitrary; in what follows, this third eigenvector is designated as the *characteristic vector* of the IPS.

Properties of an IPS can be restated as follows:

1. One lattice plane direction, (hkl), the direction of the lamellae boundaries, *i.e.*, the IP, is identical in both kinds of lamellae; that is, (hkl) has the same orientation and the same repeat distances *within* it in both lattices. However, d_{hkl} is not the same.
2. One lattice direction, $[pqr]$, direction of the characteristic vector, is also common to the two lattices, but barring identity, the repeat distance along $[pqr]$ is not the same in the two lattices. The ratio of these repeat distances is the eigenvalue associated to the characteristic vector and is also the ratio of the (hkl) spacings in the two lattices.

There is no reason, in general, for (hkl) and $[pqr]$ to be rational.

Consider a lattice plane in real space, (mno), which contains the characteristic vector $[pqr]$. Neither the direction nor the spacing of (mno) are affected by the IPS, or, in other words, (mno), has the same direction and spacing in the two types of lamellae. Therefore, in reciprocal space, reciprocal points mno coincide for the two lattices. All such points define a plane P* through 000 which is perpendicular to $[pqr]$. The two reciprocal lattices are therefore related by an IPS, the IP of which is P*.

Consider now, in real space, lattice planes (hkl) parallel to the IP. The (hkl) spacing is not the same in the two lamellae. In reciprocal space, the two corresponding hkl points lie on a line perpendicular to the (hkl) plane. The direction of this line is the direction of the characteristic vector of the IPS in reciprocal space.

The relationship between direct and reciprocal lattices for the two types of lamellae is shown in Figure B1.

Appendix C: Determination of Composition of Cryptoperthite Lamellae from Two (h0l) Spacings

Figure 7 is the Mohr circle for elastic strain, constructed from numerical values in Eqs. 3 and 5; we can measure from it that

$$\frac{1}{X - X^0}\frac{\delta d(\bar{2}04)}{d(\bar{2}04)} = -0.0095\ (-0.0087), \qquad \text{(C1a)}$$

$$\frac{1}{X - X^0}\frac{\delta d(\bar{2}01)}{d(\bar{2}01)} = +0.0137\ (+0.0146), \qquad \text{(C1b)}$$

where $d(h0l)$ is the $(h0l)$ spacing and $\delta d(h0l)$ is the change in spacing due to elastic strain.

Because variations in spacing, whether elastic or compositional, are small compared to the values of these spac-

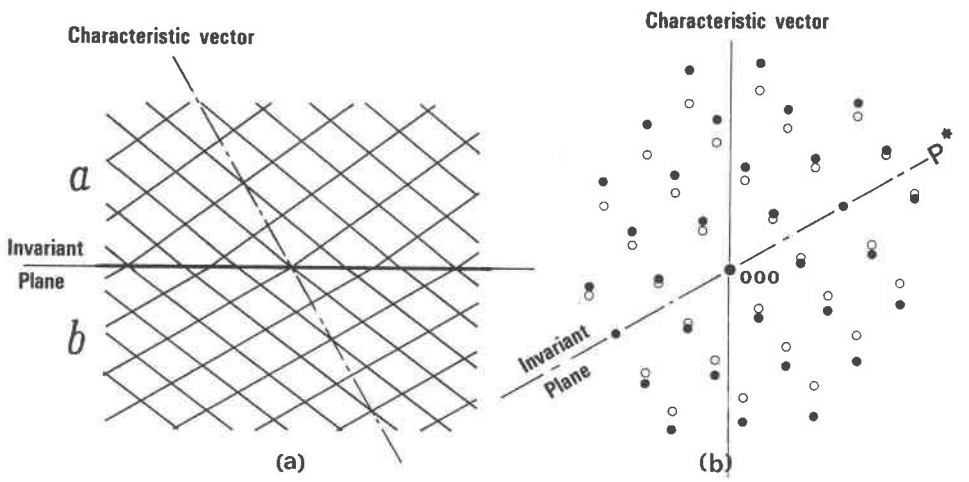

FIG. B1. Two-dimensional representation of the invariant plane strain (IPS) relating the two lattices across a coherent interface.

(a) Direct space. The plane of the interface is invariant in the linear transformation which relates one lattice to the other. The direction of the characteristic vector is that of the one lattice direction which has the same orientation in the two lattices.

(b) Reciprocal space. ○: reciprocal lattice point of phase *a*. ●: reciprocal lattice point of phase *b*. The line segments joining two reciprocal points of same index in *a* and *b* are all parallel to each other and perpendicular to the invariant plane in real space.

If the lines drawn in direct space are taken to represent directions of the vectors defining the primitive lattice cell, note that the invariant plan and the characteristic vector both have simple rational indices; this is not necessarily so in a real situation.

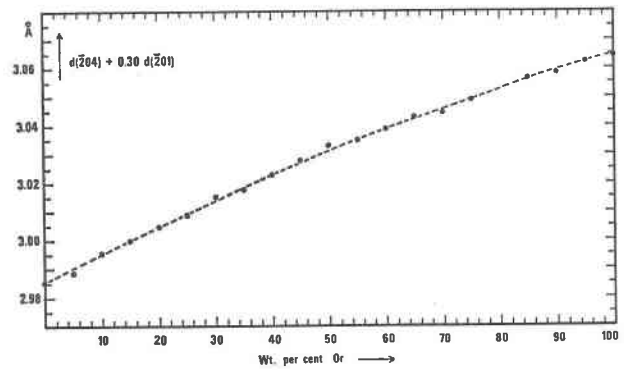

FIG. C1. Determinative parameter for anomalous cryptoperthites. This linear combination of two lattice spacings is not affected by the elastic strain due to coherency. When the two spacings are known, their linear combination can be calculated and the corresponding composition read from the curve. The coefficient in the linear combination depends to some extent on which elastic constants are held to be true; the elastic constants chosen here are those of R&A's crystal No. 61. Lattice spacing data are from Orville (1967 Table 3C).

ings, Eqs. C1 can be combined into

$$0.0137\,\frac{\delta d(\bar{2}04)}{d^0(\bar{2}04)} + 0.0095\,\frac{\delta d(\bar{2}01)}{d^0(\bar{2}01)} = 0, \quad \text{(C2)}$$

where $d^0(h0l)$ is some average value of the $(h0l)$ spacing for high temperature alkali feldspars. Taking $d^0(\bar{2}04)/d^0(\bar{2}01) = 0.435$, Eq. C2 becomes

$$\underset{(0.26)}{\delta d(\bar{2}04) + 0.30\ \delta d(\bar{2}01)} = 0. \quad \text{(C3)}$$

The combination of lattice parameters $d(\bar{2}04) + 0.30\ d(\bar{2}01)$ is therefore not affected by the elastic strain; its value (Fig. C1) is function only of the composition of the lamella and can be used to determine that composition when the two spacings are known.

Appendix D: Expression for the Chemical Potential

By definition $\bar{\Phi} = \bar{E} - T\bar{S} + P\bar{V}$, and therefore, from Eq. 11a,

$$\mathrm{d}\bar{\phi} = \bar{S}\,\mathrm{d}T + \bar{V}\sigma_{ij}\,\mathrm{d}e_{ij} + P\,\mathrm{d}\bar{V} + \bar{V}\,\mathrm{d}P + \mu\,\mathrm{d}X.$$

The constraint on any lamella which exsolves or changes composition is that it keeps matching the average crystal in the 2-and 3-directions. In any change of composition of the coherent lamella at constant P and T we therefore have

$$\mathrm{d}e_{22} = \mathrm{d}e_{33} = \mathrm{d}e_{23} = 0,$$

Because there are no shear stresses parallel to the boundaries, we thus have

$$\bar{V}\sigma_{ij}\,\mathrm{d}e_{ij} = \bar{V}\sigma_{11}\,\mathrm{d}e_{11} = -P\,\mathrm{d}\bar{V}.$$

A variation of $\bar{\Phi}$ at constant P and T is therefore given by

$$\mathrm{d}\bar{\phi}|_{P,T} = \mu\,\mathrm{d}X,$$

hence Eq. 16.

Appendix E: Coexisting Compositions on a Coherent Solvus

Equations giving the coherent solvus are obtained from $\bar{\Phi}$ exactly as the hydrostatic solvus is obtained from $\bar{G}$ (Thompson, 1967). Coexisting compositions must satisfy the system

$$\left[\bar{\phi} - X_2\left(\frac{\partial\bar{\phi}}{\partial X_2}\right)_{P,T}\right]^a = \left[\bar{\phi} - X_2\left(\frac{\partial\bar{\phi}}{\partial X_2}\right)_{P,T}\right]^b, \quad \text{(E1a)}$$

$$\left[\bar{\phi} + X_1\left(\frac{\partial\bar{\phi}}{\partial X_2}\right)_{P,T}\right]^a = \left[\bar{\phi} + X_1\left(\frac{\partial\phi}{\partial X_2}\right)_{P,T}\right]^b. \quad \text{(E1b)}$$

Taking $\bar{\Phi}$ as given in Eq. 15, with $\bar{G}$ as in Eq. 17, Eq. E1 becomes

$$RT\ln X_1^a + X_2^{a^2}(W_1 - k) + 2X_1^a X_2^{a^2}(W_2 - W_1) = RT\ln X_1^b + X_2^{b^2}(W_1 - k) + 2X_1^b X_2^{b^2}(W_2 - W_1), \quad \text{(E2a)}$$

$$RT\ln X_2^a + X_1^{a^2}(W_2 - k) + 2X_2^a X_1^{a^2}(W_1 - W_2) = RT\ln X_2^b + X_1^{b^2}(W_2 - k) + 2X_2^b X_1^{b^2}(W_1 - W_2). \quad \text{(E2b)}$$

The system E2 is formally identical to the system of equations giving the hydrostatic solvus (Thompson, 1967, Eqs. 81).

Acknowledgments

This work was carried out at the Massachusetts Institute of Technology with the support of grants from the National Science Foundation (GA-31900) and the US Geological Survey (14-08-0001-13229); it is a part of the author's doctoral work done under the supervision of W. F. Brace.

Many thanks are due to D. L. Kolhstedt (M.I.T.) for carrying out the transmission electron microscopy. J. C. Rucklidge and O. Malik (University of Toronto) did the electron microprobe analysis. Comments and criticisms of successive versions of the manuscript by W. F. Brace, T. L. Groves, R. Hon, R. M. Stesky, J. Tullis, and D. R. Waldbaum significantly improved its presentation. Discussions with, and encouragements from, W. F. Brace, C. Goetze, D. L. Kohlstedt, and R. M. Stesky were also quite helpful.

References

ABERDAM, D., AND R. KERN (1962) Observations au microscope électronique de quelques feldspaths perthitiques. *C.R. Acad. Sci.* (Paris), **255,** 734–736.

———, ———, P. LEYMARIE, AND M. PIERROT (1964) Etude cristallographique détaillée d'une orthose cryptoperthitique. *C.R. Acad. Sci.* (Paris), **258,** 1268–1271.

ARDELL, A. J. (1968) An application of the theory of particle coarsening: the γ' precipitate in Ni-Al alloys. *Acta Metall.* **16,** 511–516.

——— (1970) The growth of gamma prime precipitates in aged Ni-Ti alloys. *Metall. Trans.* **1,** 525–534.

———, AND R. B. NICHOLSON (1966) The coarsening of γ' in Ni-Al alloys. *J. Phys. Chem. Solids,* **27,** 1793–1804.

BARTH, T. F. W. (1969) *Feldspars.* Wiley-Interscience, London.

BOLLMANN, N. W., AND H.-U. NISSEN (1968) A study of optimal phase boundaries: the case of exsolved alkali feldspars. *Acta Crystallogr.* **A24,** 546–557.

BOWEN, N. L., AND O. F. TUTTLE (1950) The system $NaAlSi_3O_8$–$KAlSi_3O_8$–H_2O, *J. Geol.* **58,** 489–511.

BROWN, W. L., C. WILLAIME, AND C. GUILLEMIN (1972) Exsolution selon l'association diagonale dans une cryptoperthite: étude par microscopie électronique et diffraction des rayons X. *Bull. Soc. franç. Minéral. Cristallogr.* **95,** 429–436.

CAHN, J. W. (1962) Coherent fluctuations and nucleation in isotropic solids. *Acta Metall.* **10,** 907–913.

CHAMPNESS, P. E., AND G. W. LORIMER (1971) An electron microscopic study of a lunar pyroxene. *Contrib. Mineral. Petrol.* **33,** 171–183.

CHRISTENSEN, N. I. (1966) Compressional wave velocities in single crystals of alkali feldspar at pressures to 10 kilobars. *J. Geophys. Res.* **71,** 3113–3116.

CHRISTIE, O. H. J. (1968) Spinodal precipitation in silicates. I. Introductory application to exsolution in feldspar. *Lithos,* **1,** 187–192.

CHRISTIE, J. M., J. S. LALLY, A. H. HEUER, R. M. FISHER, D. T. GRIGGS, AND S. V. RADCLIFFE (1971) Comparative electron petrography of Apollo 11, Apollo 12, and terrestrial rocks. *Proc. Second Lunar Science Conf.* **1,** 69–89. M.I.T. Press, Cambridge, Massachusetts.

COOMBS, D. S. (1954) Ferriferous orthoclase from Madagascar. *Mineral. Mag.* **30,** 409–427.

CRAWFORD, M. L. (1966) Composition of plagioclase and associated minerals in some schists from Vermont, U. S. A., and South Westland, New Zealand, with inferences about the peristerite solvus. *Contrib. Mineral. Petrol.* **13,** 269–294.

DELBOVE, F. (1971) Equilibre d'échanges d'ions entre feldspaths alcalins et halogènures sodi-potassiques fondus. Application au calcul des propriétés thermodynamiques de la série des feldspaths alcalins. *Bull. Soc. franç. Minéral. Cristallogr.* **94,** 456–466.

DONNAY, G., AND J. D. H. DONNAY (1952) The symmetry change in the high-temperature alkali-feldspar series. *Am. J. Sci.,* Bowen vol., 115–132.

ESHELBY, J. D. (1957) The determination of the elastic field of an ellipsoidal inclusion, and related problems. *Proc. Roy. Soc. London,* **A241,** 376–396.

EVANS, B. W. (1964) Coexisting albite and oligoclase in some schists from New Zealand. *Am. Mineral.* **49,** 173–179.

FLEET, S. G., AND P. H. RIBBE (1963) An electron-microscope investigation of a moonstone. *Philos. Mag.* **8,** 1179–1187.

———, AND ——— (1965) An electron-microscope study of peristerite plagioclases. *Mineral. Mag.* **35,** 165–176.

FRISILLO, A. L., AND G. R. BARSCH (1972) Measurement of single-crystal elastic constants of bronzite as a function of pressure and temperature. *J. Geophys. Res.* **77,** 6360–6384.

GIBBS, J. W. (1906) *The Scientific Papers of J. Willard Gibbs.* Vol. I. *Thermodynamics.* Longmans, Green, and Company.

HEUER, A. H., R. F. FIRESTONE, J. D. SNOW, H. W. GREEN, R. G. HOWE, AND J. M. CHRISTIE (1971) An improved ion thinning apparatus. *Rev. Sci. Instrum.* **42,** 1177–1184.

HIRSCH, P. B., R. A. HOWIE, R. B. NICHOLSON, D. W. PASHLEY, AND M. J. WHEELAN (1965) *Electron Microscopy of Thin Crystals.* Plenum Press, New York.

IIYAMA, J. T. (1966) Contribution à l'étude des équilibres sub-solidus au système ternaire orthose-albite-anorthite à l'aide des réactions d'échange d'ions Na-K au contact d'une solution hydrothermale. *Bull. Soc. franç. Minéral. Cristallogr.* **89,** 442–454.

KELLY, A., AND R. B. NICHOLSON (1963) Precipitation hardening. In, B. Chalmers, Ed., *Progress in Materials Science,* Vol. 10. The Macmillan Company, New York.

KOREKAWA, M., H.-U. NISSEN, AND D. PHILLIP (1970) X-ray and electron-microscopic studies of a sodium-rich low plagioclase. *Z. Kristallogr.* **131,** 418–436.

LAVES, F. (1951) Relationships between exsolved plagioclase and its host (abstr.). *Am. Crystallogr. Assoc. Meet.,* Washington, D.C.

——— (1952) Phase relations of the alkali feldspars, II. *J. Geol.* **60,** 549–574.

LORIMER, G. W., AND P. E. CHAMPNESS (1973) Combined electron microscopy and analysis of an orthopyroxene. *Am. Mineral.* **58,** 243–248.

LUTH, W. C., AND O. F. TUTTLE (1966) The alkali feldspar solvus in the system Na_2O–K_2O–Al_2O_3–SiO_2–H_2O. *Am. Mineral.* **51,** 1359–1373.

———, P. M. FENN, AND R. F. MARTIN (1970) Thermodynamic excess functions, relative activities, and solvus relations for synthetic alkali feldspars (abstr.). *Geol. Soc. Am. 83rd Annu. Meet.,* Milwaukee.

———, R. F. MARTIN, AND P. M. FENN (1972) The peralkaline alkali feldspar solvus (abstr.). *Feldspar Conf. Progr.,* Manchester.

MACKENZIE, W. S., AND J. V. SMITH (1956) The alkali feldspars: III. An optical and X-ray study of high-temperature feldspars. *Am. Mineral.* **41,** 405–427.

MOORHOUSE, W. W. (1959) *The Study of Rocks in Thin Section.* Harper and Row, New York.

MUIR, I. D., AND J. V. SMITH (1956) Crystallization of feldspars in larvikites. *Z. Kristallogr.* **107,** 182–195.

MÜLLER, G. (1971) Der Einfluss der Al Si-Verteilung auf die Mischungslücke des Alkalifeldspäte. *Contrib. Mineral. Petrol.* **34,** 73–79.

NABARRO, F. R. N. (1940) The strains produced by precipitation in alloys. *Proc. Roy. Soc. London,* **A175,** 519–538.

NYE, J. F. (1957) *Physical Properties of Crystals.* Oxford University Press, London.

OFTEDAHL, C. (1948) Studies on the igneous rock complex of the Oslo region. XI. The feldspars. *Skr. Norske Vidensk.-Akad. Oslo I Mat.-Naturvidensk,* **3,** 1–77.

ORVILLE, P. M. (1963) Alkali ion exchange between vapor and feldspar phases. *Am. J. Sci.* **261,** 201–237.

——— (1967) Unit-cell parameters of the microcline-low albite and the sanidine-high albite solid solution series. *Am. Mineral.* **52,** 55–86.

RIBBE, P. H. (1960) X-ray and optical investigation of peristerite plagioclases. *Am. Mineral.* **45,** 626–644.

ROBIN, P.-Y. F. (1974a) Thermodynamic equilibrium across a coherent interface in a stressed crystal. *Am. Mineral.* **59,** 1286–1298.

——— (1974b) Angular relationships between host and exsolution lamellae and the use of the Mohr circle. *Am. Mineral.* (in press)

ROBINSON, P., H. W. JAFFE, M. ROSS, AND C. KLEIN, JR. (1971) Orientation of exsolution lamellae in clinopyroxenes and clinoamphiboles: considerations of optimal phase boundaries. *Am. Mineral.* **56,** 909–939.

RYZHOVA, T. V. (1964) The elastic properties of plagioclase. *Bull. (Izv.) Acad. Sci. USSR, Geophys. Ser.,* 1049–1051. [*Am. Geophys. Union Transl.,* 633–635.]

———, AND K. S. ALEKSANDROV (1965) The elastic properties of potassium-sodium feldspars. *Bull. (Izv.) Acad. Sci. USSR, Geophys. Ser.* 98–102. [*Am. Geophys. Union Transl.,* 53–56.]

SIMMONS, G. (1964) Velocity of compressional waves in various minerals at pressures to 10 kilobars. *J. Geophys. Res.* **69,** 1117–1121.

SMITH, J. V. (1961) Explanation of strain and orientation effects in perthites. *Am. Mineral.* **46,** 1489–1493.

———, AND W. S. MACKENZIE (1958) The alkali feldspars. IV. The cooling history of high-temperature sodium-rich feldspars. *Am. Mineral.* **43,** 872–889.

———, AND I. D. MUIR (1958) The reaction sequence in larvikite feldspars. *Z. Kristallogr.* **110,** 11–20.

SOKOLNIKOFF, I. S. (1956) *Mathematical Theory of Elasticity,* 2nd ed. McGraw-Hill Book Co., Inc., New York, 476 p.

STEWART, D. B., AND DORA VON LIMBACH (1967) Thermal expansion of low and high albite. *Am. Mineral.* **52,** 389–413.

THOMPSON, J. B., JR. (1967) Thermodynamic properties of simple solutions. In, P. H. Abelson, Ed., *Researches in Geochemistry II.* John Wiley and Sons, New York, p. 340–361.

———, AND D. R. WALDBAUM (1968) Mixing properties of sanidine crystalline solutions: I. Calculations based on ion-exchange data. *Am. Mineral.* **53,** 1965–1999.

———, AND ——— (1969) Mixing properties of sanidine crystalline solutions: III. Calculations based on two-phase data. *Am. Mineral.* **54,** 811–838.

TUTTLE, O. F. (1952) Origin of the contrasting mineralogy of extrusive and plutonic rocks. *Am. J. Sci.* **60,** 107–124.

———, AND N. L. BOWEN (1958) Origin of granite in the light of experimental studies in the system $NaAlSi_3O_8$–$KAlSi_3O_8$–SiO_2–H_2O. *Geol. Soc. Am. Mem.* **74,** 153 p.

VISWANATHAN, K., AND E. EBERHARD (1968) The peristerite problem. *Schweiz. Mineral. Petrogr. Mitt.* **48,** 803–814.

VOIGT, W. (1928) *Lehrbuch der Kristallphysik,* Teubner, Leipzig and Berlin.

WALDBAUM, D. R., AND J. B. THOMPSON, JR. (1968) Mixing properties of sanidine crystalline solution: II. Calculations based on volume data. *Am. Mineral.* **53,** 2000–2017.

———, AND ——— (1969) Mixing properties of sanidine crystalline solutions: IV. Phase diagrams from equations of state. *Am. Mineral.* **54,** 1274–1298.

WAYMAN, C. M. (1964) *Introduction to the Crystallography of Martensitic Transformations.* The MacMillan Company, New York.

WILLAIME, C. (1973) *Interprétation par des Calculs d'Énergie Élastique des Textures Observées par Microscopie Électronique dans les Cryptoperthites.* Thèse de Doctorat d'État ès Sciences. Université de Paris VI, Paris, France.

———, AND W. L. BROWN (1972) Explication de l'orientation des interfaces dans les exsolutions des feldspaths, par un calcul d'énergie élastique. *C. R. Acad. Sci. (Paris),* **275,** 627–629.

———, AND M. GANDAIS (1972) Study of exsolution in alkali feldspars. Calculation of elastic stresses inducing periodic twins. *Phys. Stat. Sol.* **A9,** 529–539.

———, W. L. BROWN, AND M. GANDAIS (1973) An electron-microscopic and X-ray study of complex exsolution textures in a cryptoperthitic alkali feldspar. *J. Mat. Sci.* **8,** 461–466.

WRIGHT, T. L., AND D. B. STEWART (1968) X-ray and optical study of alkali feldspar, I. Determination of composition and structural state from refined unit-cell parameters and $2V$. *Am. Mineral.* **53,** 38–87.

YUND, R. A., AND R. H. MCCALLISTER (1970) Kinetics and mechanisms of exsolution. *Chem. Geol.* **6,** 5–30.

Manuscript received, August 9, 1973; accepted for publication, July 24, 1974.